ARMY RESEARCH LABORATORY

Low-cost, High Performance Avalanche Photodiodes for Enabling High Sensitivity Bio-fluorescence Detection (Final Report)

by Anand V. Sampath and Michael Wraback

ARL-TR-5981 **April 2012**

NOTICES

Disclaimers

The findings in this report are not to be construed as an official Department of the Army position unless so designated by other authorized documents.

Citation of manufacturer's or trade names does not constitute an official endorsement or approval of the use thereof.

Destroy this report when it is no longer needed. Do not return it to the originator.

Army Research Laboratory
Adelphi, MD 20783-1197

ARL-TR-5981 **April 2012**

Low-cost, High Performance Avalanche Photodiodes for Enabling High Sensitivity Bio-fluorescence Detection (Final Report)

Anand V. Sampath and Michael Wraback
Sensors and Electron Devices Directorate, ARL

REPORT DOCUMENTATION PAGE

Form Approved
OMB No. 0704-0188

1. REPORT DATE *(DD-MM-YYYY)*	2. REPORT TYPE	3. DATES COVERED (From - To)
April 2012	DRI	October 2009 to October 2011

4. TITLE AND SUBTITLE
Low-cost, High Performance Avalanche Photodiodes for Enabling High Sensitivity Bio-fluorescence Detection (Final Report)

5a. CONTRACT NUMBER

5b. GRANT NUMBER

5c. PROGRAM ELEMENT NUMBER

6. AUTHOR(S)
Anand V. Sampath and Michael Wraback

5d. PROJECT NUMBER

5e. TASK NUMBER

5f. WORK UNIT NUMBER

7. PERFORMING ORGANIZATION NAME(S) AND ADDRESS(ES)
U.S. Army Research Laboratory
ATTN: RDRL-SEE-M
2800 Powder Mill Road
Adelphi, MD 20783-1197

8. PERFORMING ORGANIZATION REPORT NUMBER
ARL-TR-5981

9. SPONSORING/MONITORING AGENCY NAME(S) AND ADDRESS(ES)

10. SPONSOR/MONITOR'S ACRONYM(S)

11. SPONSOR/MONITOR'S REPORT NUMBER(S)

12. DISTRIBUTION/AVAILABILITY STATEMENT
Approved for public release; distribution unlimited.

13. SUPPLEMENTARY NOTES

14. ABSTRACT
A III-Nitride/silicon carbide (SiC) separate absorption and multiplication avalanche photodiode (SAM-APD) offers a novel approach for fabricating high gain photodetectors with tunable absorption over a wide spectrum from the visible to deep ultraviolet. However, unlike conventional heterojunction SAM-APDs, the formation of a polarization-induced charge at the heterointerface arising from spontaneous and piezoelectric polarization can dramatically affect the performance of this detector. In this report, we discuss the role of this interface charge on the performance of gallium nitride (GaN)/SiC SAM-APDs through simulations of the electric field profile within this device structure and experimental results on fabricated APDs. These devices exhibit a low dark current below 0.1 nA before avalanche breakdown and high avalanche gain in excess of 1000 with active areas 25 times larger than that of state-of-the-art GaN APDs. A responsivity of 4 A/W was measured at 365 nm when biased near avalanche breakdown.

15. SUBJECT TERMS
Ultraviolet detector, avalanche photodiodes, GaN, SiC

16. SECURITY CLASSIFICATION OF:			17. LIMITATION OF ABSTRACT	18. NUMBER OF PAGES	19a. NAME OF RESPONSIBLE PERSON
a. REPORT	b. ABSTRACT	c. THIS PAGE			Anand V. Sampath
Unclassified	Unclassified	Unclassified	UU	26	19b. TELEPHONE NUMBER (*Include area code*) (301) 394-0104

Contents

List of Figures **iv**

Acknowledgments **v**

1. Statement of the Army Problem **1**

2. Objectives **1**

3. Approach **1**

4. Experimental Methods **3**

5. Results **3**

5.1 Modeling 3

5.2 GaN/SIC APD Devices 9

6. Conclusions **14**

7. References **15**

8. Transitions **16**

Distribution List **18**

List of Figures

Figure 1. Device structure of a III-Nitride/SiC APD. 2

Figure 2. Band diagram of a GaN/SiC APD under reverse bias, with the electric field either showing punch-through into the GaN absorption region (left), or confined in the SiC multiplication region (right) due to the presence of polarization induced charge σ at the interface. 4

Figure 3. Calculation of the electric field distribution in the GaN absorption region and SiC multiplication region as a function of reverse bias for various densities of interface charge. 5

Figure 4. Calculation of the electric field and band diagram in a GaN/SiC SAM-APD accounting for spontaneous polarization charge for the case where the GaN layer is compressively strained (top), a PICCL is employed (middle), and an aluminum nitride (AlN) ICCL is employed (bottom). An exploded view of the heterointerface for each case is shown to the right. 7

Figure 5. SEM micrograph of a fabricated GaN/SiC SAM-APD. 9

Figure 6. Measured dark current (blue) and photocurrent (red) for a 130-μm-diameter GaN/SiC APD. The dark current for a typical SiC APD is shown in green. 9

Figure 7. Measured photoresponse from APD with 10-nm-thick PICCL at varying reverse bias. 10

Figure 8. Measured photoresponse from APD with 15-nm-thick PICCL at varying reverse bias. 10

Figure 9. Calculated effective carrier concentration vs. depletion width for APD15. 11

Figure 10. Calculated photoresponse for SiC detector with a GaN filter (black) based upon the photoresponse of a SiC detector (brown) and the transmission of the GaN filter (green). 11

Figure 11. Calculated (solid pink) and measured (pink open circles) total photoresponse for APD15 biased at 157 V. Calculated SiC (blue) and GaN (green) photoresponse at same reverse bias. 12

Figure 12. Calculated gain for APD15. 14

Figure 13. Calculated hole injection efficiency for APD15. 14

Acknowledgments

We gratefully acknowledge the support of Dr. Paul Shen (RDRL-SEE-M) in modeling the effects of interface polarization charge on III-Nitride/silicon carbide (SiC) avalanche photodiodes (APDs), Mr. Ryan Enck (RDRL-SEE-M) and Dr. Chad Gallinat for the growth and characterization of some of these structures, and Mr. Paul Rottella Jr for transmission electron microscopy studies. We also acknowledge Professor J. Campbell, University of Virginia, and his doctoral students Mr. Q. Zhou and Ms. D. McIntosh, for technical discussion as well as the fabrication and characterization of these devices.

INTENTIONALLY LEFT BLANK.

1. Statement of the Army Problem

Ultraviolet (UV) light-induced fluorescence-based biosensors, like the Tactical-Biological (TAC-BIO) platform under development by Edgewood Chemical and Biological Center (ECBC), are designed as low-cost, compact, robust, and energy efficient sensors to be deployed as a network of point sensors providing real-time early warning to troops on the battlefield. A major problem for the fielding of such sensors is use of photomultiplier tube (PMT) detectors, which are expensive and fragile, and operate at high voltages. Possible alternatives, including UV-enhanced silicon (Si) avalanche photodiodes (APDs) or silicon carbide (SiC) APDs, have excessive dark current, poor detectivity, or non-optimal spectral range.

2. Objectives

We propose to fabricate low dark current, high quantum efficiency, low noise, semiconductor-based single photon counting detectors in the 300 to 550 nm spectral range to replace PMTs currently employed in bio-fluorescence detection. These novel detectors will be separate absorption and multiplication avalanche photodiodes (SAM-APDs) that combine high quantum efficiency gallium nitride (GaN) (300 to 360 nm) and indium gallium nitride (InGaN) (360 to 550 nm) absorbers with the proven low dark current, low noise SiC multiplication regions inherent to photon counting Geiger mode SiC APDs to achieve performance comparable to PMTs while reducing cost and improving deployability.

3. Approach

We have fabricated SAM-APDs that employ high quantum efficiency and spectrally tunable (In)GaN in the absorption region and proven low noise, low dark current SiC in the multiplication region. The basic device is a top illuminated structure designed for pure hole injection and multiplication consisting of a heavily doped p+-SiC layer, followed by a lightly doped ν-SiC multiplication layer; an unintentionally doped ν- (In)GaN absorber; and a thin, heavily doped, n^+-GaN layer, as shown in figure 1. The (In) GaN layers are deposited by plasma-assisted molecular beam epitaxy on commercially purchased SiC epilayers/substrates. This design has significant advantages that include the possibility of having high quantum efficiency (QE) over a widely tunable spectral range from the visible to the deep UV by modifying the composition of the direct band gap III-Nitride absorption region, as well as low dark current and high gain associated with the high quality SiC multiplication region. In addition, this device

structure benefits from the formation of a type II heterojunction between the III-Nitride and 4H SiC layers with both the conduction and valence band energies of the GaN below those of the SiC and conduction band and valence band offsets that are between –0.6 and –0.9 eV and 0.7 and 1 eV, respectively (*1*). This band alignment promotes hole injection and inhibits electron injection from GaN into SiC, enabling single carrier injection of the photo-generated holes in the absorbing region into the SiC multiplication layer that is optimal since the hole ionization coefficient of SiC is much greater than that of the electron. As a result, these devices may have lower noise than SiC APDs.

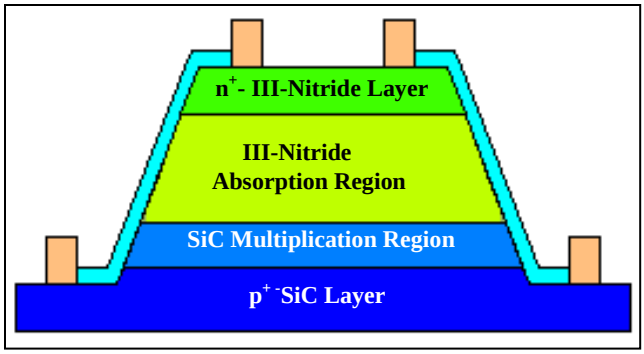

Figure 1. Device structure of a III-Nitride/SiC APD.

However, unlike traditional heterojunction SAM-APDs such as InGaAs/indium phosphide (InP) telecommunications devices, these detectors employ polar materials, with the SiC multiplication region having smaller spontaneous polarization than the III-Nitride absorption region. While the positive polarization charge expected to form at the heterointerface between (In)GaN and SiC for III-face growth can achieve an optimal electric field profile in this device, a high field in the multiplication region of the structure desirable for high gain, a low field within the absorption region, and insufficient or excessive charge can lead to poor performance. As a result, an additional method for controlling the density of interface charge is desirable.

Furthermore, InGaAs/InP APDs benefit from lattice matching of these materials as well as the ability to epitaxially grow the InP multiplication region and InGaAs absorption region directly on an InP substrate without interruption at the heterointerface; in this manner, the formation of deleterious defects can be prevented. In contrast, GaN has a 3.4% lattice mismatch with 4H-SiC that increases with InN mole fraction, resulting in the formation of threading dislocations that can act as leakage paths that increase dark current and prevent avalanche breakdown. While various heteroepitaxial buffer schemes have been developed for the growth of III-Nitrides on SiC, these approaches must be modified or preferably avoided since the SiC region is not simply a substrate and the success of these devices hinges upon the efficient collection of photogenerated holes in the SiC multiplication region.

This program has focused on the growth and fabrication of the GaN/SiC SAM-APDs and understanding the impact of the functional heterointerface on realizing APDs with low dark current. These interface issues include the role of polarization-induced charge, the role of strain,

and the impact of defects arising from heteroepitaxy including dislocation density and impurities. These issues are addressed through modeling of both theoretical devices structure as well as the performance of fabricated devices.

4. Experimental Methods

The structure of the fabricated GaN/SiC APDs consists of a 2-μm-thick p+-SiC layer having acceptor concentration of $2x10^{18}$ cm^{-3}, a 480-nm-thick n-SiC multiplication layer unintentionally doped $5x10^{15}$ cm^{-3}, a 300-nm-thick n-GaN layer unintentionally n-type doped GaN absorption layer, and a 10- to 50-nm-thick n^+-GaN layer doped $2x10^{18}$ cm^{-3}. The SiC epitaxial layers were grown on Si- face 4H-SiC substrates and purchased from Cree Inc. The III-polar GaN epitaxial layers were heteroepitaxially grown by plasma assisted molecular beam epitaxy at 850 °C directly upon the SiC epitaxial layers without the use of traditional buffer layers. The role of polarization-induced interfaced charge is investigated by employing a similarly doped p-type GaN interface charge control layer (PICCL) between the SiC multiplication region and GaN absorption region with thicknesses of 10 and 15 nm that will be referred to as APD10 and APD15, respectively. The SiC substrates were chemically prepared prior to growth by solvent cleaning and RCA cleaning as described previously (*2*). The substrate is prepared in-situ immediately prior to growth by periodically covering the epitaxial surface with gallium (Ga) metal and then allowing the metal to desorb as described by Korakakis et al. (*3*).

The DC photoresponse of these devices was measured by illuminating the detector using a broad spectrum laser diode light source lamp. The optical power was held nearly constant over the spectral range using a motor-controlled variable neutral density (ND) filter. Capacitance-voltage (C-V) measurements were taken using an Agilent 4284 LCR meter using a 100-kHz AC bias with amplitude of 500 mV.

5. Results

5.1 Modeling

The relationship between the electric field at the heterointerface between (In)GaN and SiC and the polarization-induced charge is given by Gauss' Law, which can be expressed for this case as

$$\varepsilon_{SiC} E_{SiC} = \varepsilon_{GaN} E_{GaN} + \sigma_n , \quad (1)$$

where E_{SiC}, E_{GaN}, ε_{SiC}, and ε_{GaN} are the electric field and dielectric constant in the SiC multiplication and GaN absorption regions, respectively, and σ_n is the net interface charge density. As we demonstrate, σ_n strongly impacts the electric field distribution in this device and

therefore detector performance. Consider the case of the detector structure shown in figure 1 under large reverse bias V_b just short of avalanche breakdown. Neglecting the contributions from the band offset between GaN and SiC and the space charge in the p+ and n+ regions, the applied voltage may be expressed as

$$E_{SiC}d_{SiC} + E_{GaN}d_{GaN} = V_b\,, \tag{2}$$

where d_{SiC} and d_{GaN} are the thickness of the depletion region in the n$^-$ SiC and n^- GaN layers, respectively.

Equations 1 and 2 can be solved for the distribution of the electric field in the SiC multiplication region and the GaN absorption region, which can be expressed as

$$\begin{cases} E_{GaN} = \dfrac{\varepsilon_{SiC}V_b - \sigma_n d_{SiC}}{\varepsilon_{GaN}d_{SiC} + \varepsilon_{SiC}d_{GaN}} \\ E_{SiC} = \dfrac{\varepsilon_{GaN}V_b + \sigma_n d_{GaN}}{\varepsilon_{GaN}d_{SiC} + \varepsilon_{SiC}d_{GaN}} \end{cases}. \tag{3}$$

However, these expressions are only valid for the case where

$$V_b > \frac{\sigma_n}{\varepsilon_{SiC}}d_{SiC}\,. \tag{4}$$

Then the electric field can punch-through into the GaN absorption region, as illustrated in the band diagram in figure 2 (left). For the circumstances where equation 4 is not satisfied, a two-dimensional electron gas (2DEG) forms in the GaN at the heterointerface to offset σ_n, as shown in figure 2 (right), and the electric field in the GaN and SiC regions are instead given by

$$\begin{cases} E_{GaN} = 0 \\ E_{SiC} = \dfrac{V_b}{d_{SiC}} \end{cases} \tag{5}$$

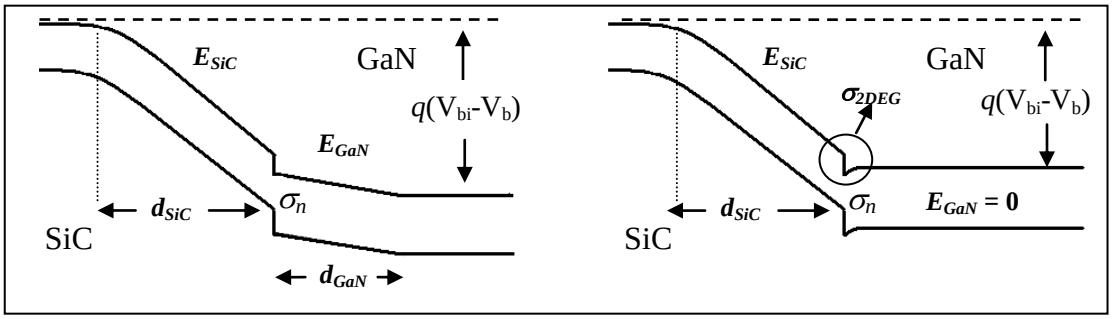

Figure 2. Band diagram of a GaN/SiC APD under reverse bias, with the electric field either showing punch-through into the GaN absorption region (left), or confined in the SiC multiplication region (right) due to the presence of polarization induced charge σ at the interface.

Figure 3 shows the calculated electric field in the GaN absorption and SiC multiplication regions as a function of applied bias for a number of net interface charge densities. At small reverse bias, the electric field is confined entirely within the SiC layer. When the applied bias satisfies the condition in equation 4, punch-though occurs and $E_{GaN} \neq 0$. It is clear from figure 3 that increasing interface charge increases the bias required to achieve punch-through. However the critical field in the SiC multiplication region (E_{SiC}^{cr}), beyond which avalanche breakdown occurs, places an upper limit on the applied reverse bias. As a result, excessive interface charge makes it impossible to extend the electric field to the GaN region prior to avalanche breakdown within the SiC multiplication region, thus reducing the QE of the detector by limiting charge collection to a primarily diffusion mechanism in the absorption region. In contrast, insufficient charge will lead to excessive electric field in the absorber region, resulting in increased injection of background carriers from the absorption region into the multiplication region, and therefore higher dark current. For an optimized device, the electric field in the SiC multiplication region should approach but not exceed E_{SiC}^{cr} , while the electric field in the GaN absorption region should be non-zero, but less than the breakdown field for GaN (E_{GaN}^{br}), i.e.,

$$\begin{cases} 0 < E_{GaN} < E_{GaN}^{br} \\ E_{SiC} \approx E_{SiC}^{cr} \end{cases}. \tag{6}$$

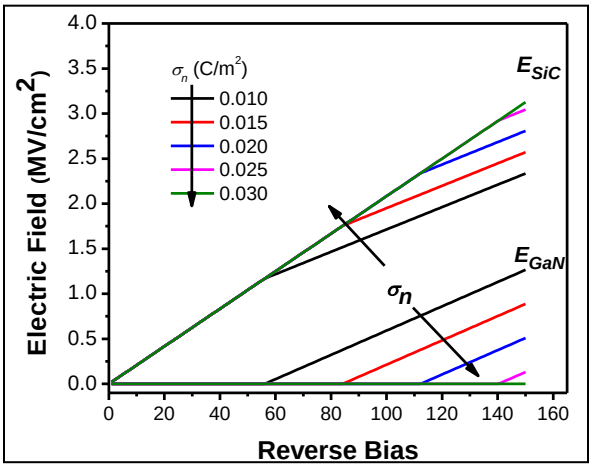

Figure 3. Calculation of the electric field distribution in the GaN absorption region and SiC multiplication region as a function of reverse bias for various densities of interface charge.

To It can be shown that inequality (equation 6) requires

$$\varepsilon_{SiC} E_{SiC}^{cr} - \varepsilon_{GaN} E_{GaN}^{br} < \sigma_n < \varepsilon_{SiC} E_{SiC}^{cr} . \tag{7}$$

It is important to note that $E_{GaN}^{br} << E_{SiC}^{cr}$ for heteroepitaxially grown GaN due to the presence of a large dislocation density at the heterointerface that has been demonstrated to give rise to large leakage currents at low reverse bias in GaN p-n junction diodes. As a result, equation 7

indicates that the parameter space for optimal interface charge density, so that the detector can have both high QE and low dark current, is narrower in this case.

To appreciate the role of polarization-induced interface charge in practice, consider the specific case of a GaN/ 4H-SIC APD structure consisting of a 480-nm-thick n-type SiC multiplication region doped ~$5x10^{15}$ cm^{-3} that has been demonstrated to yield low dark current SiC APDs (*4*) and a 300-nm-thick n-type GaN layer doped ~$1x10^{16}$ cm^{-3}, so as to have nearly full absorption above the bandgap of GaN in the absorption region for high QE. The net interface charge in this detector is calculated to be between ~0.013 – 0.023 C/m^2 , using ~0.034 C/m^2 as the spontaneous polarization in GaN (*5*) and 0.011 – 0.021 C/m^2 for 4H-SiC, based upon the work of Bai et al. (*6*). The net interface charge may be excessive for the lower estimate of the spontaneous polarization for 4H-SiC, therefore preventing punch-through prior to avalanche breakdown in this detector (figure 2, right).

One approach to controlling the interface charge in this device is to employ strain engineering, since GaN is a piezoelectric material. Compressive strain in the GaN absorption region can reduce the net interface charge by inducing a piezoelectric charge with opposite sign to that of the spontaneous polarization charge, while tensile strain will increase the net interface charge. Figure 4 (top) shows the calculated electric field profile for the GaN/SiC SAM-APD biased just short of avalanche breakdown and assuming the GaN layer is compressively strained (–0.24). This strain state induces a piezoelectric charge that reduces the net interface charge to ~0.1 C/m^2, thus allowing punch-through prior to avalanche breakdown.

An alternative approach is to introduce charge at the interface through dopants. This interface charge control layer (ICCL) can contain ionized acceptors or donors to provide negative or positive charge, respectively. To illustrate this concept, figure 4 (middle) shows the calculated electric field distribution in a GaN/SiC APD employing a 2-nm magnesium (Mg)-doped PICCL at the heterointerface that introduces a negative interface charge density of 0.11 C/m^2. This charge is sufficient to allow punch-through of the electric field into the GaN absorption region, but also introduces a small barrier for hole transport into the SiC multiplication region (figure 4 middle).

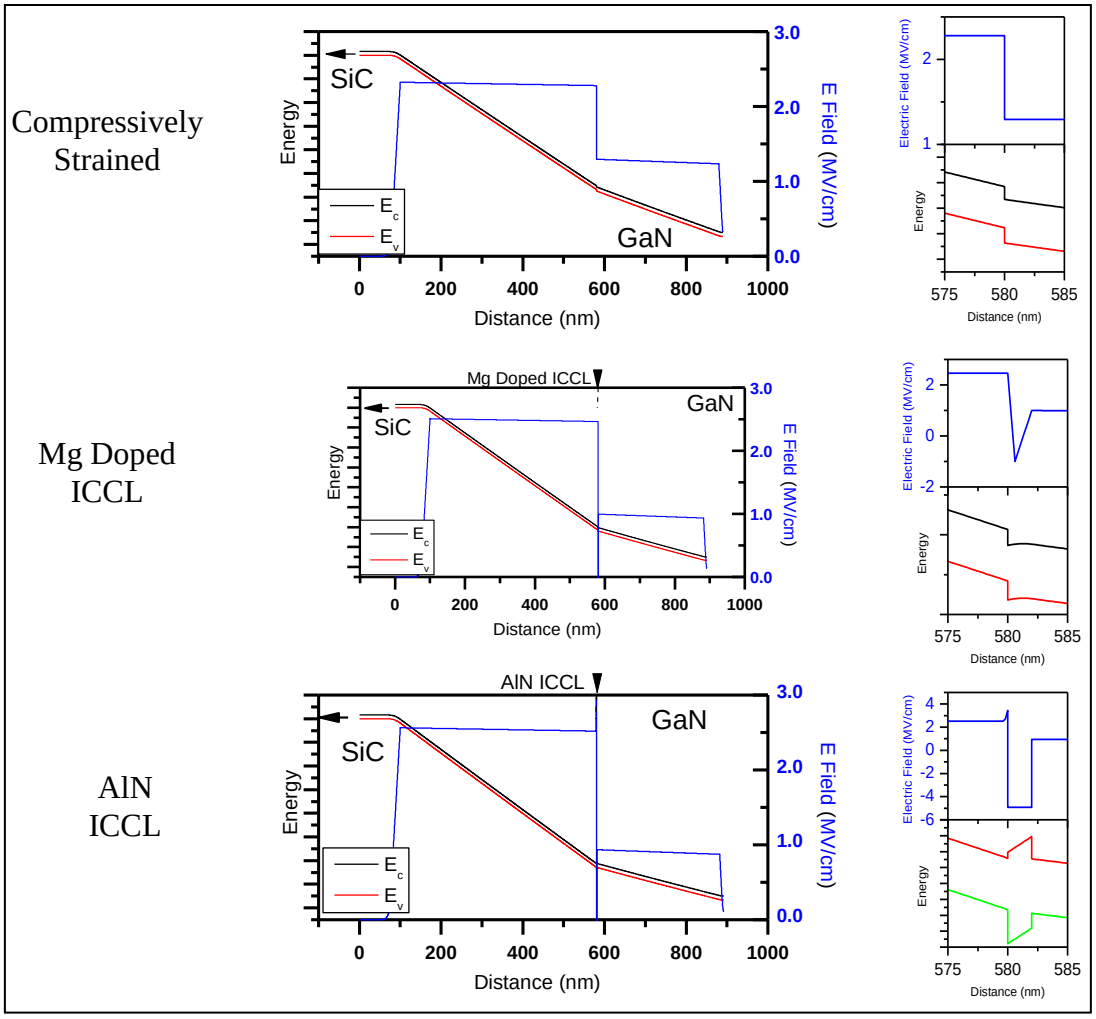

Figure 4. Calculation of the electric field and band diagram in a GaN/SiC SAM-APD accounting for spontaneous polarization charge for the case where the GaN layer is compressively strained (top), a PICCL is employed (middle), and an aluminum nitride (AlN) ICCL is employed (bottom). An exploded view of the heterointerface for each case is shown to the right.

A third approach is to introduce a layer having larger spontaneous polarization than the absorption or multiplication region, for example, an AlN ICCL. This charge control layer introduces a type I band alignment between AlN and SiC that creates a 2DEG in the SiC multiplication region and a two-dimensional hole gas (2DHG) in the GaN absorption region, as shown in figure 4 bottom, with the effect of reducing the net interface charge density. However, the AlN ICCL also introduces a significant barrier for hole transport into the SiC multiplication region that may reduce carrier collection efficiency. This barrier may be reduced by employing an AlGaN ICCL having lower spontaneous polarization than AlN but still having sufficient bandgap energy so as to maintain a type-I band alignment and a dipole at the heterointerface.

While SAM-APDs fabricated in other materials systems, such as indium gallium arsenide (InGaAs)/InP SAM APDs, require little electric field in the absorption region to achieve high QE

because of large carrier diffusion lengths to collect carriers, GaN/SiC SAM APDs likely cannot employ this approach due to the large density of dislocations that arise at heterointerface resulting from lattice mismatch. In addition, since the interface between the SiC multiplication region and the GaN absorption region also coincides with the initiation of heteroepitaxial growth, the presence of surface impurities may act in concert with extended defects to further increase the probability of hole trapping at the interface and reduce detector QE. While dislocation densities as low as 10^8 cm^{-3} have been reported in GaN when employing a thin AlN buffer (*7*) or substrate patterning, these approaches may be undesirable due to the need for hole transport across the heterointerface for collection. Instead, the presence of an electric field to decrease the transit time of photogenerated holes into the SiC multiplication region is likely essential to reduce the probability of trapping and obtain high QE.

The requirement for optimizing the net interface charge density to ensure a desirable low electric field in the III-Nitride absorption region should depend strongly upon the composition of the absorption region, which will affect both spontaneous and piezoelectric polarization. For the case of a GaN/SiC SAM-APD, residual tensile strain, which arises from the larger thermal expansion coefficient of GaN (5.59 x10^{-6}/K) over that of SiC (~4.20 x10^{-6}/K) despite the smaller *a* lattice constant of 4H-SiC (3.07 A) over GaN (3.18 A), should lead to an increase in σ_n over what would be expected for a fully relaxed structure. This strain can be managed by reducing the growth temperature or introducing an AlN buffer layer, which has been found to change the strain state in the GaN epilayer to compressive (*8*) and could therefore potentially provide an avenue for reducing the net interface charge. However, as discussed previously, the formation of the 2DEG in the SiC that would also result in lower net interface charge density must also be taken into account so as not to increase the electric field in the GaN so much that dark current also increases. For a deep UV AlGaN/SAM-APD, the high AlN mole fraction absorption region will have larger spontaneous polarization that will likely result in an increase in net interface charge over a GaN/SiC SAM-APD, in conjunction with the reduction in strain due to the closer lattice match between AlN and 4H-SiC. While the spontaneous polarization component of the interface charge in InGaN/SiC SAM APDs operating in the visible would likely be similar to that of a GaN/SiC SAM APD, the piezoelectric component arising from tensile strain may be significantly higher in the former, depending upon the degree of relaxation that would occur. Thus, it is apparent that the use of an interface charge control layer provides an additional degree of control over the net charge density that allows for tailoring the electric field in the detector for optimal performance.

While this discussion treats the case of a GaN/SiC SAM-APD structure designed for the multiplication of holes, and therefore, employing a net positive interface charge, inverse arguments, including inversion of the crystal polarity to N-face, apply for a device designed for electron multiplication. In this case, the formation of a negative polarization charge is desirable. An important example of this case would be a III-N/Si (111) APD, which would require a p-type, N-polar III-Nitride contact layer and an unintentionally doped N-polar absorption region for

efficient electron collection. Such devices are complicated by the observation that III-Nitride materials grown on Si (111) are reported to be III-polar as grown. More generally, these arguments can be applied to any SAM-APD structure composed of a multiplication and absorption region having unequal total polarization.

5.2 GaN/SIC APD Devices

Figure 5 shows a scanning electron micrograph (SEM) of a typical fabricated APD employing a beveled sidewall to reduce the magnitude of the electric field along the circumference of the device with respect to the bulk so as to avoid premature breakdown. These devices are top illuminated through a silicon dioxide (SiO_2) passivation layer and electrically contacted using a titanium (Ti)/Al/nickel (Ni)/gold (Au) ohmic metal ring contact on the top n-GaN layer and a Ni/Ti/Al/Ni ohmic contact to the p-SiC layer (not visible in SEM image). These APDs exhibit dark currents as low as 0.1 nA near breakdown for a 130-μm-diameter device independent of the ICCL thickness (figure 6, black curve) that is similar to what is observed for comparable SiC APDs (figure 6, green curve), and devices with diameters up to 250 μm have been demonstrated. This result suggests that the reverse leakage currents in these devices are limited by the SiC multiplication region despite the presence of threading dislocations at the heterointerface. It is also important to note that the dark current in these devices is ~1000 times lower than what has been observed for GaN APDs despite having areas that are up to ~25 times larger.

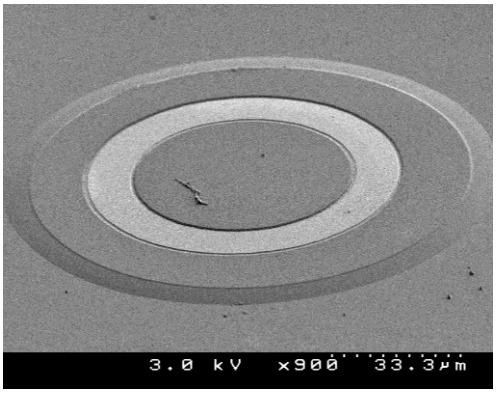

Figure 5. SEM micrograph of a fabricated GaN/SiC SAM-APD.

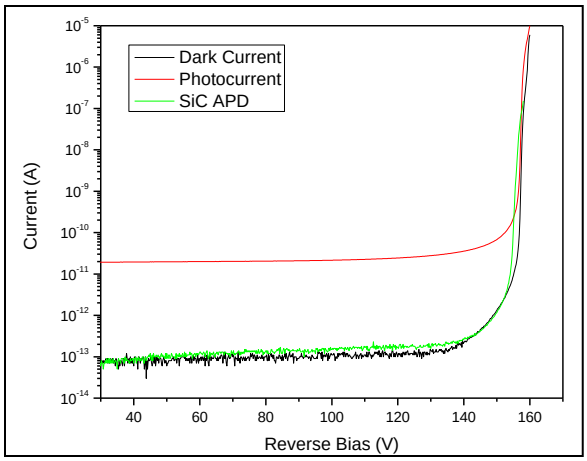

Figure 6. Measured dark current (blue) and photocurrent (red) for a 130-μm-diameter GaN/SiC APD. The dark current for a typical SiC APD is shown in green.

The photoresponse as a function of reverse bias measured for APD 10 is shown in figure 7. These devices exhibit a local peak unity gain responsivity of 2.13 mA/W at ~372 nm at 70-V reverse bias. The responsivity increases with reverse bias above ~100-V bias due to gain in the multiplication region. The shape of the response is constant with increasing reverse bias and exhibits a local maxima at ~372 nm and a local minima at ~365 nm that is inconsistent with a

typical GaN or SiC photodetector. In addition, the response is nearly flat in the deep UV region ($\lambda < 280$ nm) in contrast to what is typically observed for SiC or GaN photodetectors.

The photoresponse as a function of reverse bias measured for APD15 is shown in figure 8. These devices exhibit a peak unity gain responsivity of 0.69 mA/W at ~374 nm. The shape of the response is consistent with that of APD10 at low reverse bias. However, this shape changes with increasing reverse bias and is consistent with GaN response when biased near avalanche breakdown, above ~159 V. Similar to APD10, the deep UV response of these devices is either flat or slightly increasing at all reverse bias. A responsivity of ~4.0 A/W was measured at 364 nm for a reverse bias of 161 V.

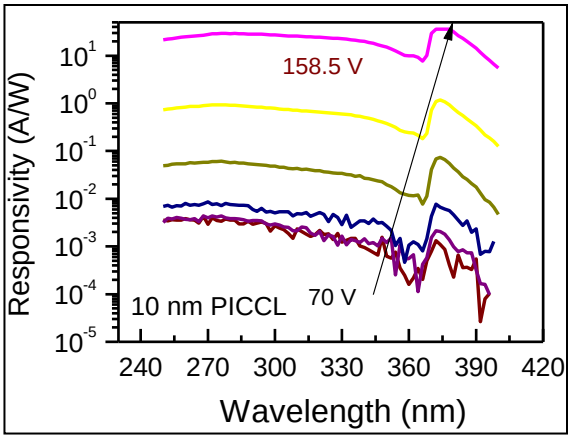

Figure 7. Measured photoresponse from APD with 10-nm-thick PICCL at varying reverse bias.

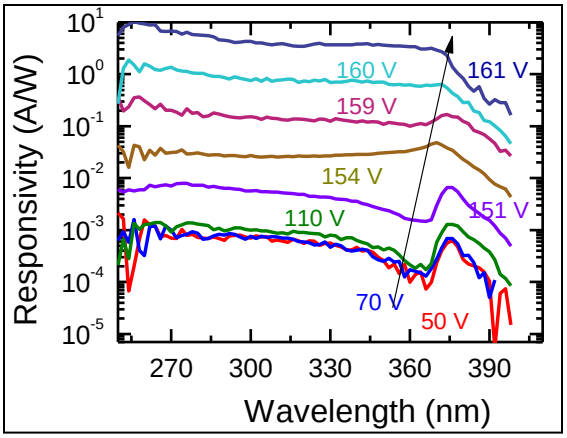

Figure 8. Measured photoresponse from APD with 15-nm-thick PICCL at varying reverse bias.

Figure 9 shows the calculated carrier concentration as a function of depletion width based on C-V measurements for APD15. An effective carrier concentration of $4\text{x}10^{17}$ cm^{-3} is found for APD 15 at low reverse bias and softly transitions to ~$3\text{x}10^{16}$ cm^{-3} at ~130-V reverse bias.

The origins of the observed spectral response can be understood by analyzing the components of the photocurrent in these devices. Since GaN has a wider bandgap than SiC and because of incomplete absorption in the GaN absorption region, the photoresponse has a component associated with carrier generation in the SiC multiplication region (R_{SiC}) in addition to the current associated with the generation and injection of holes from the GaN absorption region (R_{GaN}). The total photoresponse can then be expressed as

$$R_{photo} = R_{SiC} + R_{GaN}\,. \tag{8}$$

The SiC component of the photoresponse will be a function of photon wavelength and reverse bias and may be expressed as

$$R_{SiC}(V,\lambda) = \frac{\left(1-R_{\mathrm{Re}\,f}\right)q}{\hbar\nu} \bullet e^{-\alpha(\lambda)d_{GaN}} \bullet \eta_{SiC}(\lambda) \bullet g(V)\,, \tag{9}$$

where R_{Ref} is the reflectance of the illuminated surface, η_{SiC} is the QE of the SiC acting as an absorption region, α and d are the absorption coefficient and thickness of the GaN absorption region, and g is the gain in the SiC multiplication region. The product of the first and second term of equation 9 is the net photon flux incident upon the SiC region accounting for reflection at the illuminated surface and transmission through the GaN absorption region.

The GaN component of the photoresponse is given by

$$R_{GaN}(V,\lambda) = \frac{(1-R_{\mathrm{Re}\,f})q}{\hbar\nu} \bullet e^{-\alpha(\lambda)(d_{GaN}-d_{depl})} \bullet \left(1-e^{-\alpha(\lambda)d_{depl}}\right) \bullet \eta_{inj}(V) \bullet g(V), \qquad (10)$$

where d_{depl} is the thickness of the depletion in the GaN absorption region and η_{inj} is the hole injection efficiency from the GaN into the SiC layer. The contribution of diffusion to the GaN photocurrent is neglected in equation 3 due to short hole diffusion length expected in this material that results from a high defect density. The product of the first and second terms of equation 10 is the incident photon flux on the depleted GaN absorption region.

Figure 10 shows the calculated SiC related photoresponse using equation 9. The quantum efficiency of SiC, η_{SiC}, was measured using wholly SiC p-i-n APD structures having a 480-nm-thick intrinsic region (the dashed curve). The transmission through the Ga N absorption region was calculated using the absorption coefficient given by reference 9 and assuming a thickness of 480 nm similar to what was employed for the fabricated APDs. Unity gain was assumed the calculated photocurrent is to that measured for APD10 at 70-V bias. The calculated I_{SiC}, figure10 brown curve, exhibits a minima at ~365 nm and a maxima at ~374 nm that is consistent with what is observed for APD10 as well as APD15 at low bias. This result indicates that photoresponse for these devices is entirely related to the generation of carriers in the SiC multiplication region, and the GaN related photocurrent is negligible. However, equation 9 cannot on its own explain the change in response shape observed in APD15 with increasing bias.

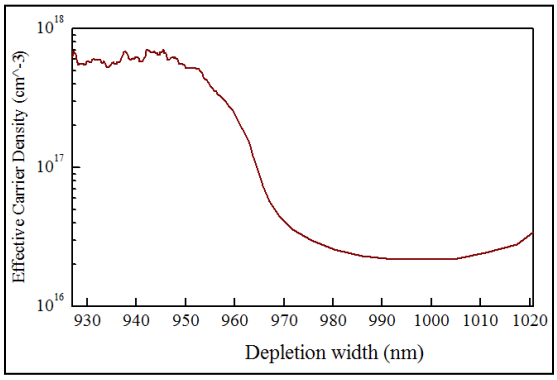

Figure 9. Calculated effective carrier concentration vs. depletion width for APD15.

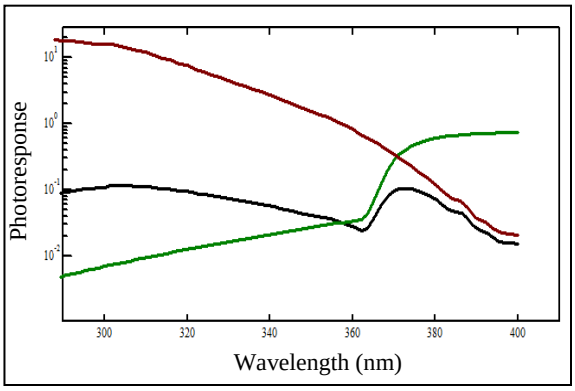

Figure 10. Calculated photoresponse for SiC detector with a GaN filter (black) based upon the photoresponse of a SiC detector (brown) and the transmission of the GaN filter (green).

Figure 11 shows the calculated and measured total photoresponse in an APD biased at 157. In addition to the SiC component (blue sold line), the GaN component of the photocurrent (green solid line) is calculated from equation 10 where the depletion region thickness, hole injection efficiency, and gain are fit to the experimentally measured data. The measured calculated total response (pink solid line) agrees well with the calculated response (pink open circles), indicating that the GaN contribution to the photoresponse is responsible for the change in shape observed for APD15 in figure 8. This result indicates that punch-through of the electric field into the GaN absorption region and a non-zero depletion region thickness is required for the collection of holes photo-generated within.

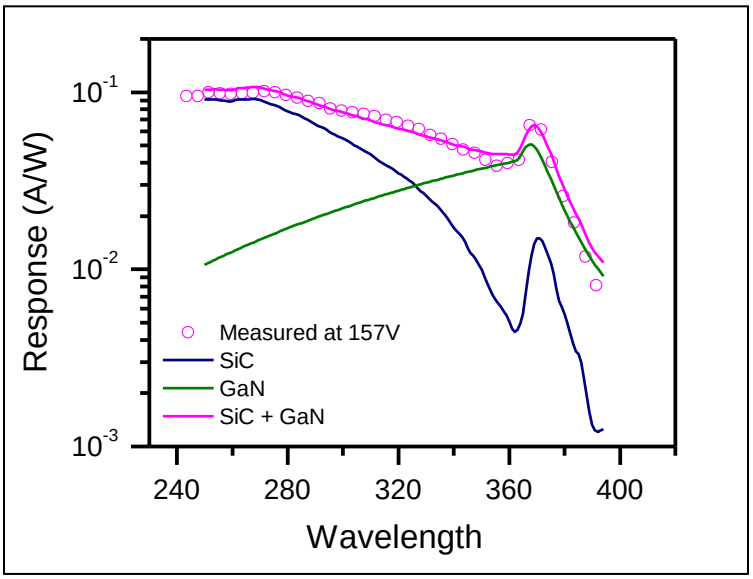

Figure 11. Calculated (solid pink) and measured (pink open circles) total photoresponse for APD15 biased at 157 V. Calculated SiC (blue) and GaN (green) photoresponse at same reverse bias.

This suggests that the electric field in APD10, which shows no GaN response prior to avalanche breakdown, does not punch-through into the GaN absorption region. This conclusion is supported by C-V measurements (not shown). In contrast, measurements of APD15 show a similar carrier concentration for bias up to 130 V that is consistent with initially depleting the p-SiC region. However, increasing the reverse bias results in a reduction in the effective carrier concentration to ~$3x10^{16}$ cm^{-3} that better reflects the background doping in the unintentionally doped GaN absorption regions and indicates punch-through of the electric field into this layer. It is important to note that this relatively high carrier concentration results in a non-instantaneous depletion of the absorption region that introduces another dependence of the GaN photocurrent with increasing reverse bias that accounts for the gradual recession of the valley in the photoresponse observed at 365 nm for these devices (figure 8).

The disparate behavior between APD10 and APD15 may be explained by the difference in net charge at the heterointerface. As discussed in the previous section, excessive interface charge

will contain the electric field in the APD to the multiplication region and prevent punch-through prior to avalanche breakdown. As a result, holes photogenerated in GaN absorption region must diffuse rather than drift into the SiC multiplication region; negligible GaN photocurrent is generated in this manner due to the short diffusion lengths in this layer arising from defects generated by heteroepitaxy as demonstrated by APD10. However, the net interface charge can be optimized through the use of a PICCL through the relation

$$\sigma_{net} = \sigma_{pol} - N_A d_{PICCL} \tag{11}$$

for the case where σ_{net} and σ_{pol} are the net and positive polarization induce interface charge densities, and N_A and d_{PICCL} are the acceptor concentration and thickness of the PICCL layer. Then increasing the PICCL thickness to 15 nm sufficiently offsets the positive polarization induced interface charge so as to allow punch-through in APD15 prior to avalanche breakdown.

Conventionally, the gain in an APD is calculated from the unity gain response by

$$G(V_b) = \frac{I_{photo}(V_b) - I_{dark}(V_b)}{I_{photo}(V_{G=1}) - I_{dark}(V_{G=1})}, \tag{12}$$

where G is the gain at reverse bias V_b and the dark (I_{dark}) and photocurrent (I_{photo}) are measured at V_b and at a voltage corresponding to unity gain. Using this expression, these devices exhibit gain in excess of 10^5 prior to avalanche breakdown. However, this expression cannot apply to the case of this GaN/SiC APD because it does not account for the different components of the photocurrent at unity, I_{SiC}, and non-unity gain, I_{SiC} and I_{GaN}, and the different net photon flux associated with each component. As a result, the gain associated with avalanche multiplication cannot be determined from equation 12. Instead, the avalanche multiplication gain from these devices is extracted from fitting the measured data to equation 8, as shown in figure 12 for APD15. These devices exhibit high gain greater than 1000 that is similar with what has been observed for wholly SiC APDs. The hole injection efficiency is also determined in this manner and shown in figure 13. The efficiency peaks at 12% under lower bias and narrow GaN depletion thickness and decreases with increasing reverse bias and wider depletion to ~3% and currently limits the performance of these devices. This reduction is responsible for the SiC component dominating the total response at wavelengths shorter than ~330 nm (figure 5) and is likely associated with the presence of defects at the heterointerface. A significant defect density in the GaN absorption region is expected due to the requirement for transport across the heterointerface that restricts common the buffer layer such as using an AlN. In addition, impurities residing at the heterointerface despite the surface preparation process may also play a role. However, it is important to note that the current peak efficiency of 12% is significantly larger than the ~3% QE exhibited by state of the art SiC APDS at 365 nm. The injection efficiency may be significantly improved by investigating methods for (1) improving the initial epitaxial surface through hydrogen or oxygen cleaning, (2) modifying growth conditions to suppress incorporation of impurities and defects, and (3) exploring new buffer layer schemes

such as AlGaN that can both reduce the formation of dislocations and provide efficient transport across the heterointerface.

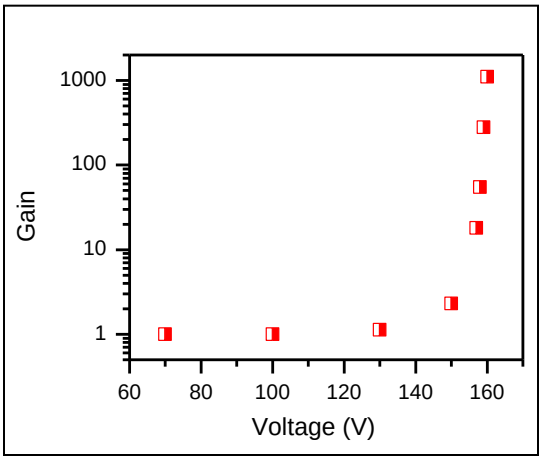

Figure 12. Calculated gain for APD15.

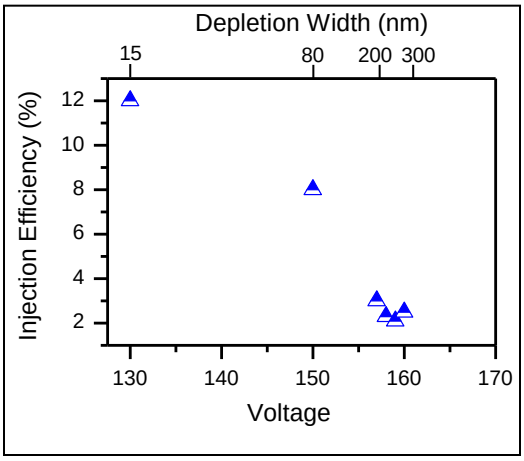

Figure 13. Calculated hole injection efficiency for APD15.

6. Conclusions

III-Nitride/SiC SAM-APDs show great promise for realization of high gain detectors that can operate over a widely tunable spectrum in the near and deep UV, where there are currently limited alternatives. Prototype GaN/SiC SAM-APDs have been demonstrated that exhibit dark currents comparable to that of SiC APDs and a peak responsivity of ~4 A/W. However, we have shown that the design and optimization of this device requires attention to the formation of interface charge that arises at the heterointerface due to the difference in spontaneous polarization of 4H-SiC and GaN, as well as to the presence of defects at the interface; the former can determine the electric field profile in the detector, and the latter establishes the range of interface charge density that can simultaneously provide high QE with low dark current. The net interface charge density may be tailored to optimize device performance by employing strain management and/or introducing an interface charge control layer doped with acceptors or having larger spontaneous polarization.

7. References

1. Danielsson, E.; Zetterling, C.-M.; Ostling, M.; Linthicum, K.; Thomson, D. B.; Nam, O.-H.; Davis, R. F. The Influence of Band Offsets on the IV Characteristics for GaN/SiC Heterojunctions. *Sol. State Electron.* **2002**, *46*, 827–35.

2. Zhou, Qiugui; McIntosh, Dion C.; Lu, Zhiwen; Campbell, Joe C.; Sampath, Anand V.; Shen, Hongen; Wraback, Michael. GaN/SiC Avalanche Photodiodes. *Appl. Phys. Lett.* **2011**, *99*, 131110.

3. Korakakis, D.; Sampath, A.; Ng, H. M.; Morales, G.; Goepfert, I. D.; Moustakas, T. D. Growth and Doping of GaN Directly on 6H-SiC by MBE. *MRS Proc*. **1996**, *395*, 151.

4. Liu, M.; Bai, X.; Hu, C.; Guo, X.; Campbell, J. C.; Pan, Z.; Tashima, M. M. Low Dark Count Rate and High Single-photon Detection Efficiency Avalanche Photodiode in Geiger-mode Operation. *IEEE Phot. Tech. Lett.* **2007**, *19*, 378–80.

5. Vurgaftman, I.; Meyer, J. R. Band Parameters for Nitrogen-containing Semiconductors. *J. Appl. Phys.* **2003**, *94*, 3675–96.

6. Bai, S.; Devaty, R. P.; Choyke, W. J.; Kaiser, U.; Wagner, G.; MacMillan, M. F. Determination of the Electric Field in 4H/3C/4H-SiC Quantum Wells Due to Spontaneous Polarization in the 4H SiC Matrix. *Appl. Phys. Lett.* **2003**, *83*, 3171–3173.

7. Tanaka, S.; Iwai, S.; Aoyagi, Y. Reduction of the Defect Density in GaN Films using Ultra-thin AlN Buffer Layers on 6H-SiC. *J. of Cryst. Growth* **1997**, *170*, 329–334.

8. Perry, W. G.; Zheleva, T.; Bremser, M. D.; Davis, R. F.; Shan, W.; Song, J. J. Correlation of Biaxial Strains, Bound Exciton Energies, and Defect Microstructures in GaN Films Grown on AIN/6H-SiC(0001) Substrates. *J. of Electron Mat.* **1997**, *26*, 224–231.

9. Muth, J. F.; Brown, J. D.; Johnson, M.A.L.; Yu, Shonghai; Kolbas, R. M.; Cook, Jr. J. W.; Schetzina, J. F. Absorption Coefficient and Refractive Index of GaN, AiN and AlGaN Alloys. MRS Internet J. Nitride Semicond. Res. 4S1, G5.2, 1999.

8. Transitions

The work from this Director's Research Intiative (DRI) produced five presentations, including four invited presentations, as well as two refereed journal papers and two patent applications filed with the United States Patent and Trademark Office over the course of the two-year program. Detailed citations are as follows:

1. Sampath, A. V.; Enck, R. W.; Shen, H.; Wraback, M.; Zhou, Q.; McIntosh, D.; Campbell, J. III-Nitride/SiC Separate Absorption and Multiplication Avalanche Photodiodes: The Importance of Controlling Polarization Induced Interface Charge. Presented at the *IEEE Lester Eastman Conference (LEC) on High Performance Devices*, Troy, NY, August 2010.
2. Wraback, M.; Sampath, A. V.; Enck, R. W.; Shen, H.; Zhou, Q.; McIntosh, D.; Campbell, J. Hybrid III-Nitride/SiC Ultraviolet Avalanche Photodiodes. Invited presentation at the *Workshop on Compound Semiconductor Materials and Devices*, Savannah, GA, February 2011.
3. Shen, H.; Sampath, A. V.; Zhou, Q.; Campbell, J.; Wraback, M. Effect of Interface Polarization Charge on GaN/SiC Separate Absorption and Multiplication Avalanche Photodiodes. Invited presentation at *2001 Electrochemical Society Meeting*, Boston, MA.
4. Sampath, A. V.; Enck, R. W.; Shen, H.; Zhou, Q.; McIntosh, D.; Campbell, J.; Wraback, M. III-Nitride/SiC Separate Absorption and Multiplication Avalanche Photodiodes. Invited presentation at *West Virginia University Graduate Student Seminar*, Morgantown, WV, October 2011.
5. Sampath, A. V.; Enck, R. W.; Shen, H.; Zhou, Q.; McIntosh, D.; Campbell, J.; Wraback, M. Impact of Hetero-interface on the Photoresponse of GaN/SiC Separate Absorption and Multiplication Avalanche Photodiodes. Invited presentation at *2011 International Semiconductor Device Research Symposium*, College Park, MD, December 2011.
6. Sampath, A. V.; Enck, R. W.; Shen, H.; Wraback, M.; Zhou, Q.; McIntosh, D.; Campbell, J. III-Nitride/SiC Separate Absorption and Multiplication Avalanche Photodiodes: The Importance of Controlling Polarization-Induced Interface Charge. *Int. J. of High Speed Electron. and Systems* **2011**, *20*, 487.
7. Zhou, Qiugui; McIntosh, Dion C.; Lu, Zhiwen; Campbell, Joe C.; Sampath, Anand V.; Shen, Hongen; Wraback, Michael. GaN/SiC Avalanche Photodiodes. *Appl. Phys. Lett.* **2011**, *99*, 131110.
8. Wraback, M.; Shen, H.; Sampath, A. V. Polarization Enhanced Avalanche Photodetector and Method Thereof, filed in the United States Patent and Trademark Office, May 2011.

9. Shen, H.; Wraback, M.; Sampath, A. V. Semiconductor Photodetector with Transparent Interface Charge Control Layer and Method Thereof, filed in the United States Patent and Trademark Office, May 2011.

NO. OF COPIES	ORGANIZATION
1 ELEC	ADMNSTR DEFNS TECHL INFO CTR ATTN DTIC OCP 8725 JOHN J KINGMAN RD STE 0944 FT BELVOIR VA 22060-6218
5	US ARMY RSRCH LAB ATTN IMNE ALC HRR MAIL & RECORDS MGMT ATTN RDRL CIO LL TECHL LIB ATTN RDRL CIO LT TECHL PUB ATTN RDRL SEE M A SAMPATH ATTN RDRL SEE M M WRABACK ADELPHI MD 20783-1197